Submission code: 0P8X8LB0PY

See this and other abstracts on our website: https://home.sbgf.org.br/Pages/resumos.php

Q-factor Inversion for Depth Migration

Claudio Cardoso (Petrobras)

Q-factor Inversion for Depth Migration

Abstract

The current new exploratory frontier in Brazil is the Equatorial Margin. Apart from the velocity building challenges represented by paleo-canions with velocity inversions, strongly structured carbonate platforms, gravitational cells with compressive components giving rise to overthrusts, mud volcanoes etc., there are shallow gas accumulations that affect seismic quality and alter AVO response. Their influence is twofold and intertwined: their shape and velocity are difficult to precisely define, causing image defocusing, and, if not corrected, attenuation effect washes out amplitudes and decreases resolution, creating shadow zones below the gas anomaly. Therefore, precisely defining Q-factor to be used in Q-compensation migration can be crucial for some exploration targets.

In this work, I briefly describe the visco-acoustic wavefield extrapolation and the computation of the gradient of the Q-inversion problem in the image space, illustrating with simple examples.

Introduction

In conventional seismic processing, Q-compensation is a twostep process: firstly, phase is corrected with respect to a central frequency and, secondly, amplitude effects are considered after migration. This scheme is acceptable if Q-factor is homogeneous. In the presence of Q-factor anomalies or with lateral variations, Q-compensation needs to consider the wave-propagation path. Migration with Q-compensation aims at dynamically and kinematically correcting the effects attenuation has on seismic data.

Inverting for the Q-factor using tomographic schemes dates back late 70's (Kjartansson, 1979). After this seminal work, several authors proposed different schemes of measuring attenuation effects on the data domain (Tonn, 1991; Quan and Harris, 1997) and using ray-tracing to project those measurements back to the model domain. Only in 2016, Yi Shen proposed a method in which residuals are determined in the image domain and their propagation uses wavefields instead of rays. She called it WEMQA, acronym of Wave-Equation Migration Q Analysis, which borrows several features from Sava and Biondo's WEMVA (2004). Here, I closely follow Shen's work, but with some tweaks.

In the theory section, I first describe the modeling and migration using the attenuative one-way wave equation and, in the following, derive the operators used in WEMQA. In the results section, I illustrate the application of WEMQA on simple but explanatory models.

Theory and Results

The Q-model considered in this work is that of Futterman (1962), in which Q is almost independent of frequency. This leads to a visco-acoustic one-way wave equation very similar to the purely acoustic one. The dispersion relation is $k_z = \sqrt{(\omega\tilde{s})^2 - \mathbf{k}^2}$, with a complex frequency-dependent slowness $\tilde{s}(\omega)$ given by (Kjartansson, 1979)

$$\tilde{s}(\omega) = s_{\omega_r}\left(1 - \frac{1}{\pi Q} ln\left(\frac{\omega}{\omega_r}\right)\right)\left(1 + \frac{i}{2Q}\right), \qquad 1$$

where s_{ω_r} is the slowness at the reference frequency ω_r, chosen to be the dominant frequency. The real part on the RHS is related to the dispersion and the imaginary part, to the absorption.

A phase-shift plus interpolation scheme is used for wavefield extrapolation. Equation 1 is unconditionally stable when used in modeling. However, since visco-acoustic migration preferentially increases the high frequency content, under some circumstances it can inadequately boost high frequency noise. Given that the more the wavefields propagate, the higher the amplitude of the high frequency noise, a depth-velocity-frequency filter is implemented.

The simple model of Figure 1 illustrates the importance of using correct physics. At the bottom of the figures, is the amplitude distribution along the six reflectors, supposedly with the same constant reflectivity. On the right, the central trace of the image is represented. The Q-model consists of a constant value of 100 everywhere and a Q-anomaly of 30 in the center as shown in the figure. As can be seen on the set on the left, acoustic migration does not correct the phase of the wavelet, nor the amplitudes. On the right, the image resulting from the visco-acoustic migration shows the correct phase and correct amplitudes.

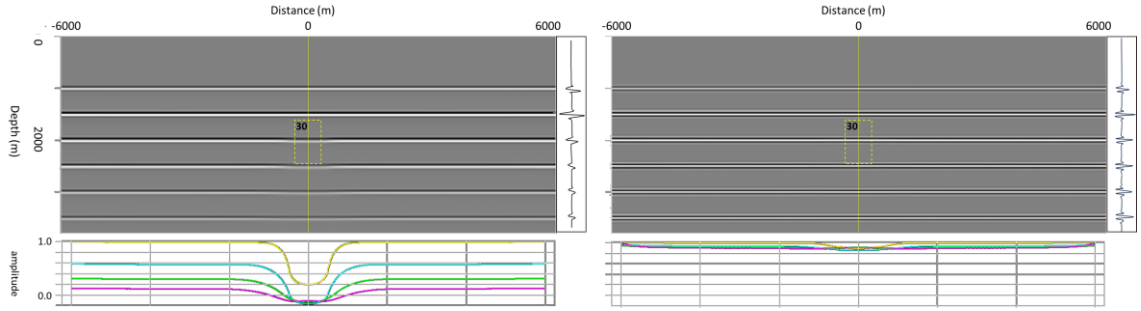

Figure 1: Images resulting from acoustic migration of visco-acoustic data (left) and visco-acoustic migration of visco-acoustic data (right).

I use the Marmousi II model (Martin et al, 2006) to illustrate the importance of using the correct Q-model (Figure 2). The correct Q-factor is 100 everywhere, except within the yellow rectangle in which it is 30. No velocity errors are present in this example. On the left is the result of visco-acoustic migration with constant Q=100. On the right, is the result of visco-acoustic migration with the correct Q-factor. Clearly, the image on the left presents attenuated amplitudes and lower resolution in a region below the Q-factor anomaly. Moreover, it is also clear that amplitude and phase distortions spread over an area which is not vertically restricted to the anomaly. Consequently, the conventional attenuation compensation would fail to recover the correct image. On the right, image with correct amplitudes and phase shows better resolution below the Q-anomaly.

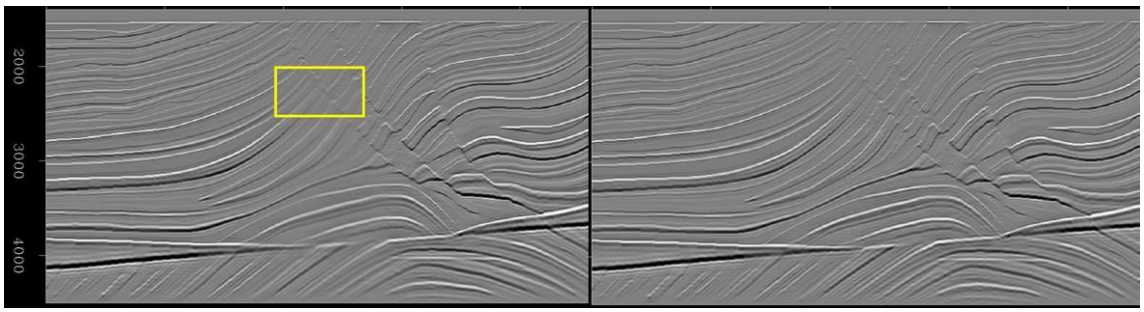

Figure 2: Images resulting from visco-acoustic migration of visco-acoustic data with Q=100 (left) and with the correct Q (right).

To estimate Q , WEMQA minimizes the objective function $J(Q) = \frac{1}{2}\|\rho(Q)\|^2$, in which the residual ρ is a measure of some characteristics of the image, which reflects some Q-inaccuracy. In the present case, the residual is computed by the Spectral Ratio Method (Tonn, 1991), for which difference between amplitude spectra measured in localized windows and reference windows is indicative of inadequately corrected attenuation. Reference windows are

defined in regions where Q-factor is expected to be correctly compensated. Here, the residuals are computed in a depth-to-time converted image to circumvent the wavelet stretch issue in depth migration.

Gradient ∇_Q of the objective function with respect to the Q-factor is

$$\nabla_Q J = \frac{\partial I}{\partial Q}^* \left[\mathcal{F}^* \left(-\frac{1}{|R_c|}\frac{1}{vk_z}\Phi\right)\rho\right], \qquad 2$$

where R_c is the amplitude spectrum and Φ is the phase spectrum of the Fourier transformed image along the depth axis, ρ is the residual is computed by the Spectral Ratio Method stretched back to depth, $\mathcal{F}^*$ is the inverse Fourier transform along the k_z axis. The first term on the RHS is the adjoint wave-equation tomographic operator, acting on the image perturbation (the term within brackets).

To illustrate the action of the tomographic operator and the adequacy of the perturbed image (term within brackets of equation 3) to solve for the Q-factor, I use again the Marmousi 2 model. Q-factor equals 100, for these computations. In Figure 3, the top left shows the action of the tomographic operator on a known Q-factor perturbation which is zero everywhere, except for inside of the rectangle, in which it is 30. The top right shows the image perturbation computed according to the bracketed term of equation 3. They look very similar, except for the fact that the image perturbation is bit laterally restricted. At the bottom left, is the action of the adjoint tomographic operator on the image of the top left, and at the bottom right, the action of the same operator on the image of the top right (which represents the gradient in equation 3). They basically display the same information.

A simple steepest descent scheme, preconditioning the gradient with smoothing, resulted in the images of Figure 4, after 3 iterations. The objective function dropped 90% from the initial value. In Figure 4, the left column shows the result of Q-factor inversion at the bottom and the corresponding image on the top. The right column shows the correct Q-factor at the bottom and the corresponding image. There is virtually no difference between the images.

Conclusions

I show the application of Shen's method on simple models to illustrate the inversion for a Q-model which minimizes a measure of the difference between the amplitude spectrum of a pre-stack migrated image and a reference spectrum at a region correctly compensated for the inaccuracy of Q-factor. In the examples, the velocity model I used is the correct one. The next steps will investigate the crosstalk between velocity and Q-factor to allow simultaneous inversion for velocity and Q-factor.

Acknowledgments

The author acknowledges Petrobras for allowing publishing this expanded abstract.

References

Futterman, W. I., 1962, Dispersive body waves: Journal of Geophysical Research, 67, 5279-5291.

Kjartansson, E., 1979, Constant Q wave propagation and attenuation: Journal of Geophysical Research, 84, 4737-4748.

Martin, G.S., R. Wiley, and K. Marfurt, 2006, Marmousi2: An elastic upgrade for Marmousi: The Leading Edge, 25(2):156-166.

Quan, Y. and J. M. Harris, 1997, Seismic attenuation tomography using the frequency shift method: Geophysics, 62, 895-905.

Sava, P. and B. Biondi, 2004, Wave-equation migration velocity analysis-I: Theory: Geophysical Prospecting, 52, 593606.

Shen, Y., B. Biondi, and R. Clapp, 2018, Q-model building using one-way wave-equation migration Q analysis — Part 1: Theory and synthetic test: Geophysics, 83, S93-S109.

Tonn, R., 1991, The determination of seismic quality factor Q from VSP data: A comparison of different computational techniques: Geophysical Prospecting, 45, 87-109.

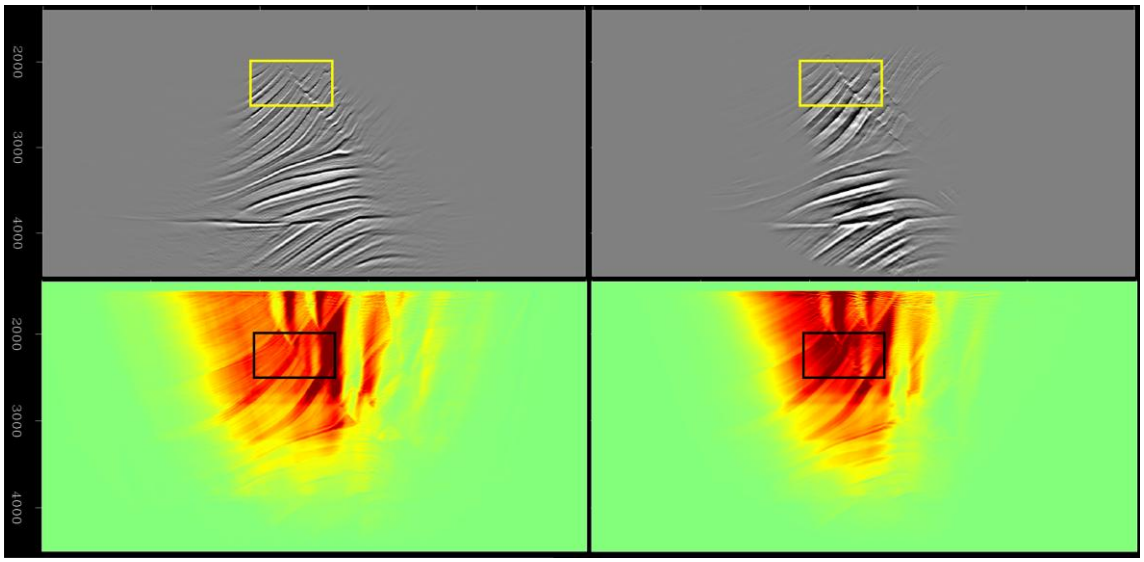

Figure 3: The left column shows the action of the tomographic operator given a known Q-factor perturbation: direct operator on top and adjoint at the bottom. The right column shows on the top the WEMQA image perturbation and at the bottom the action of the adjoint tomographic operator on it.

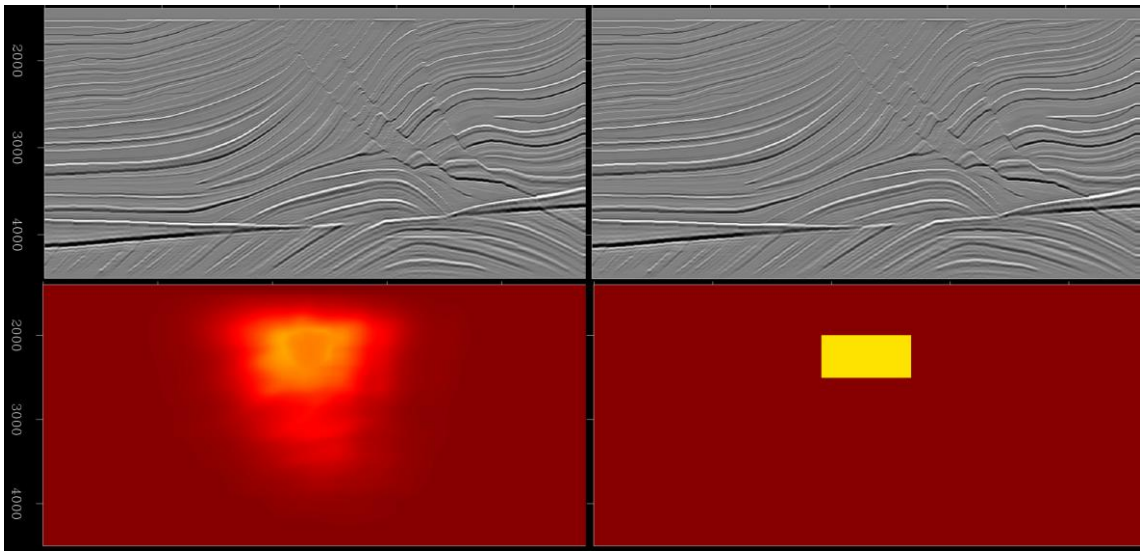

Figure 4: The left column shows the result of Q-factor inversion at the bottom and the corresponding image on the top. The right column shows the correct Q-factor at the bottom and the corresponding image. There is virtually no difference between the images.